Cross-shore transport of nearshore sediment by river plume frontal pumping

Horner-Devine, Alexander R.; Pietrzak, Julie D.; Souza, Alejandro J.; McKeon, Margaret A.; Meirelles, Saulo; Henriquez, Martijn; Flores, Raúl P.; Rijnsburger, Sabine

DOI
10.1002/2017GL073378

Publication date
2017

Document Version
Final published version

Published in
Geophysical Research Letters

AGU PUBLICATIONS

Geophysical Research Letters

RESEARCH LETTER
10.1002/2017GL073378

Key Points:
- Near-surface density fronts from Rhine River plume propagate onshore through the surf zone
- Onshore frontal propagation drives offshore flux of fine sediment
- This process generates exchange between the nearshore and the inner shelf

Correspondence to:
A. R. Horner-Devine,
arhd@uw.edu

Citation:
Horner-Devine, A. R., J. D. Pietrzak, A. J. Souza, M. A. McKeon, S. Meirelles, M. Henriquez, R. P. Flores, and S. Rijnsburger (2017), Cross-shore transport of nearshore sediment by river plume frontal pumping, *Geophys. Res. Lett.*, *44*, 6343–6351, doi:10.1002/2017GL073378.

Received 9 MAR 2017
Accepted 5 MAY 2017
Accepted article online 8 MAY 2017
Published online 28 JUN 2017

Cross-shore transport of nearshore sediment by river plume frontal pumping

Alexander R. Horner-Devine[1], Julie D. Pietrzak[2], Alejandro J. Souza[3], Margaret A. McKeon[1], Saulo Meirelles[2], Martijn Henriquez[2], Raúl P. Flores[1,4], and Sabine Rijnsburger[2]

[1]Civil and Environmental Engineering, University of Washington, Seattle, Washington, USA, [2]Department of Hydraulic Engineering, Delft University of Technology, Delft, Netherlands, [3]National Oceanography Centre, Liverpool, UK, [4]Departamento de Obras Civiles, Universidad Técnica Federico Santa María, Valparaíso, Chile

Abstract We present a new mechanism for cross-shore transport of fine sediment from the nearshore to the inner shelf resulting from the onshore propagation of river plume fronts. Onshore frontal propagation is observed in moorings and radar images, which show that fronts penetrate onshore through the nearshore and surf zone, almost to the waterline. During frontal passage a two-layer counterrotating velocity field characteristic of tidal straining is immediately set up, generating a net offshore flow beneath the plume. The seaward flow at depth carries with it high suspended sediment concentrations, which appear to have been generated by wave resuspension in the nearshore region. These observations describe a mechanism by which vertical density stratification can drive exchange of material between the nearshore region and the inner shelf. To our knowledge these are the first observations of this frontal pumping mechanism, which is expected to play an important role in sediment transport near river mouths.

Plain Language Summary The processes that exchange sediment, contaminants, or other materials between the shallow wave-influenced region very near the shoreline and deeper coastal waters are not well understood, in part because this interface is a boundary between regions where very different processes dominate. This paper illustrates a mechanism that enables exchange across this interface that involves an interesting interplay between wave processes that dominate close to the shoreline and the intrusion of buoyant river water that is circulating offshore.

1. Introduction

The surf zone is thought to form a semipermeable barrier that can limit the cross-shore exchange of water borne contaminants, sediments, and organisms between offshore waters and the shoreline [*Grant et al.*, 2005; *Rilov et al.*, 2008; *Shanks et al.*, 2010; *Ohlmann et al.*, 2012]. The mechanisms that engender exchange between the surf zone and offshore coastal waters remain poorly understood. Waves [*Reniers et al.*, 2010] and cross-shore winds [*Fewings et al.*, 2008; *Lentz and Fewings*, 2012] have both been found to be important for cross-shelf transport. In this work we describe a new exchange mechanism in which tidally generated fronts from the Rhine River outflow propagate onshore and drive suspended sediment from the nearshore region 2–3 km offshore.

Traditionally, nearshore sediment transport processes are thought to be barotropic [*Stive and Battjes*, 1984; *Fredsøe and Deigaard*, 1992], deriving energy for sediment suspension from the wavefield and transport from the wave-induced velocity field, whereas sediment transport in estuaries is often strongly influenced by baroclinic processes [e.g., *Burchard et al.*, 2013; *de Nijs et al.*, 2010]. In coastal regions of freshwater influence (ROFI) near river mouths, both wave- and buoyancy-driven transport processes are likely to be important. However, little is known about the interaction between these processes, partly because they are not expected to co-occur; strong vertical density stratification is not expected to survive in the energetic nearshore region.

The Rhine River ROFI, or plume, extends most of the length of the Dutch coast, significantly affecting the dynamics in the inner shelf region due to tidal straining [*Souza and Simpson*, 1996; *De Boer et al.*, 2009] and alongshore advection [*De Boer et al.*, 2008]. Tidal motions form freshwater lenses that are ejected from the river mouth during ebb tide propagate out over the plume and are eventually incorporated into it [*de Ruijter et al.*, 1997]. The dynamics of these freshwater lenses, and especially the fronts that bound them, are similar to

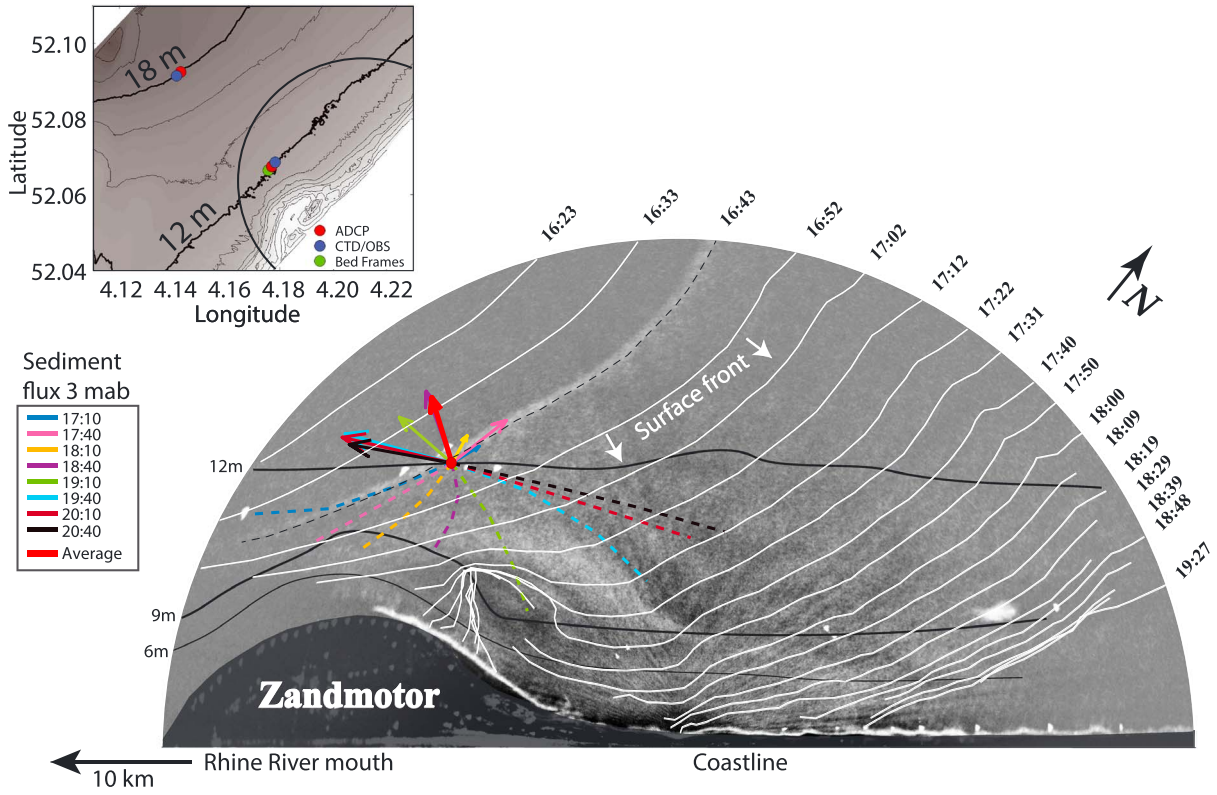

Figure 1. Radar image at 16:43 on day 57, when the front is passing the 12 m mooring location (see dashed black line in Figure 3). The red dot indicates the mooring location. The dashed black line and white lines show the front location at 16:43 and at other times. The colored arrows indicate the magnitude and direction of near-bottom sediment flux at the indicated times, and the dashed lines indicate the approximate origin of that sediment based on integration of the velocity backward in time for 30 min. The solid black lines are the 6 m, 9 m, and 12 m isobaths. Inset: bathymetric map of the 12 m and 18 m mooring locations and the field of view of the radar imaging (black semicircle).

the tidal plume fronts described in other systems [*Garvine*, 1974; *Kilcher and Nash*, 2010; *Horner-Devine et al.*, 2015]. Stratification associated with the Rhine ROFI has a large impact on the distribution of sediment along the coast, as well as contributing sediment when the river is in flood [*Pietrzak et al.*, 2011].

2. Methods

The STRAINS (STRAtification Impacts on Nearshore Sediment transport) experiment involved the deployment of two moorings along the Dutch coast, approximately 10 km northeast of the mouth of the Rotterdam waterway, through which much of the Rhine River discharges. The STRAINS experiment was motivated by the need for an improved understanding of sediment transport processes along the Dutch coast as a result of mandating of the coastal turbidity levels associated with an extension to the Port of Rotterdam at the Rhine River mouth, as well as a massive experimental beach nourishment project, referred to as the Sand Engine [*Stive et al.*, 2013]. The mooring locations are immediately seaward of the Sand Engine and 10 km from the Port of Rotterdam (Figure 1).

The moorings were deployed in 12 m and 18 m water depths, corresponding to 2 km and 6.5 km from the shoreline (Figure 1). Profiles of salinity, temperature, velocity, and suspended sediment concentration (SSC) were measured at both sites using a combination of CTD (conductivity-temperature-depth), ADCP (acoustic Doppler current profiler), and OBS (optical backscatter) instruments. The CTD and OBS instruments at the 12 m site were mounted 1, 4, 6, 9, and 11 m and 1, 6, 7, and 9 m below the surface, respectively. These instruments had sampling frequencies between 0.07 and 1 Hz, and the data were subsequently averaged into 10 min bins.

The OBS instruments were precalibrated to standard formazin solutions, and the data were converted to mass concentrations using a 1.1 mgL^{-1} formazin turbidity $unit^{-1}$ conversion based on over 400 bottle samples gathered by the Port of Rotterdam in this region of the Dutch coastal waters. The Port of Rotterdam

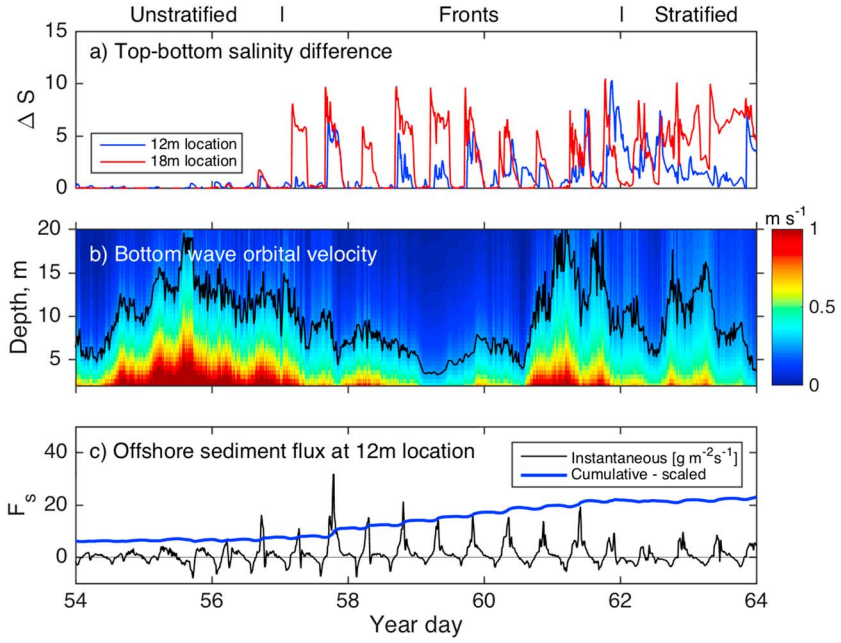

Figure 2. (a) Salinity at the 12 m and 18 m moorings, (b) bottom orbital velocity based on linear wave calculation, and (c) instantaneous and cumulative sediment fluxes at the 12 m mooring. The black line in Figure 2b shows the 0.25 ms^{-1} resuspension threshold for fine sand. The cumulative flux in Figure 2c has been scaled for plotting (*y* axis units are equal to 60 kg m^{-2}) and represents the sum of the instantaneous fluxes since the beginning of the experiment on day 43.

calibration value captures a very wide range of conditions and thus represents a good estimate of mean conditions. Seasonal and other variability in the system will result in variability in the optical response of the suspended sediment. *van der Hout et al.* [2015] report that the optical response varied by as much as a factor of 2 when they compared results from the Dutch coast spanning 8 years. For this reason, the mass concentrations reported here provide a robust measure of the variability of SSC over the course of the experiment but need to be considered in the context of the expected calibration variability when compared with concentrations from other studies.

The ADCP sampled at 1 Hz in 0.25 m vertical bins and was also averaged into 10 min bins. Wave statistics were measured with a Waverider buoy located 1 km to the southwest of the 12 m mooring. Bottom stresses due to waves and tidal currents were estimated using the measured bottom currents, wave height, period, and direction based on the formulation by *Grant and Madsen* [1979].

3. Results

3.1. Conditions

The moorings were deployed from 23 February to 7 March 2013 (year days 43 to 66), capturing almost two spring-neap cycles. During this time the Rhine discharge was 2200 $m^3\ s^{-1}$, approximately equal to the annual mean. Wind was consistently from the northeast, with a speed of approximately 3 to 7 ms^{-1} toward the beginning and end of the experiment and with a pronounced peak exceeding 12 ms^{-1} centered on day 54 in the middle of the experiment. The upwelling-favorable wind event mixed the plume and forced the freshwater offshore and to the south of the moorings, resulting in uniform top-to-bottom salinity with a value typical of coastal conditions (32 practical salinity unit (psu)) outside the Rhine ROFI at both the 12 m and 18 m sites from days 53 to 57 (Figure 2a). After the wind event, the ROFI penetrated northward into the measurement region on each flood tide. The frontal passage events are most intense from days 57 to 62 and are marked in the salinity record by a sudden drop of 5–10 psu in less than 1 min in the top 3 to 5 m at both the 18 m and 12 m sites. We refer to this as the frontal period, which is followed by a period of more persistent stratification (Figure 2a).

The significant wave height was between 0.5 m and 1 m at the beginning and end of the experiment and peaked at almost 2 m on day 56. Wave period varied between 4 s and 5 s, except after day 59 when it increased to between 6 s and 8 s. The bottom wave orbital velocity estimated for each possible water depth based on a linear wave model and the wave buoy data are shown in Figure 2b.

3.2. Cross-Shore Suspended Sediment Transport

We define the near-bottom cross-shore suspended sediment flux F_s as the product of the measured sediment concentration 3 m from the bottom and the average cross-shore velocity 2–4 m from the bottom. The cross-shore transport at the 12 m mooring during the measurement period was dominated by intense pulses of seaward transport in the bottom half of the water column (Figure 2c). These sediment pulses occurred primarily during the frontal period (days 57–62) and were timed with each frontal passage (Figure 2a). During the frontal period, the offshore transport pulses were more than 4 times higher than the onshore pulses, resulting in a net offshore transport (Figure 2c). Cross-shore transport rates during the 5 day frontal period were significantly higher than any other period during the 23 day deployment and accounted for more than 65% of the total transport. Transport during an earlier frontal period (not shown) accounted for an additional 20% of the total, suggesting that as much as 85% of the net near-bottom cross-shore transport occurred during frontal periods. By comparison, there was very little cross-shore transport at depth during the unstratified storm period (Figure 2c; days 54–56) despite high winds and waves. Below we investigate the mechanism leading to the high cross-shore transport rates during the frontal period and the source of the sediment that is transported offshore.

We observe that fronts, which are initially angled at 45° to the coast, propagate alongshore and toward the coast, rotating toward the coast over the course of the tide (Figure 1). The detailed dynamics during a single frontal passage event are shown in Figure 3. The arrival of the front at the mooring location is indicated by a sudden drop of more than 5 psu in the surface salinity (Figure 3a). The cross-shore velocity profile develops strong vertical shear almost immediately upon arrival of the front; the average velocity in the surface plume layer (0 to 3 m below the surface) is 0.4 ms^{-1} shoreward, and the velocity beneath the plume is 0.2 ms^{-1} seaward (Figure 3b). The arrival of the front is also accompanied by elevated suspended sediment concentrations (SSC), which lag the frontal arrival by approximately 0.5 h (Figure 3d). The combination of elevated seaward velocity and sediment concentration in the lower water column results in a spike in the near bed (Figure 3f) and depth averaged (not shown) seaward sediment transport initiated by the frontal passage. The elevated SSC and offshore sediment flux is concentrated in the 8 m thick layer beneath the plume. While the initiation of the sediment pulse is sudden, the shear and the associated seaward flux of sediment persist for 5–6 h each day. Cross-shore transport is much lower when the water column is unstratified before and after the passage of the front and plume (Figure 3f).

The flow-field and sediment transport induced by the front is dynamic and three dimensional, with counter-rotating elliptical motions induced in the surface and lower layers (Figure 3c). Immediately prior to the arrival of the front the velocity over the entire water column is almost exactly parallel to the coast. As the front passes, the surface flow rotates anticyclonically (clockwise) toward shore generating onshore velocity and the lower layer flow rotates cyclonically away from shore generating seaward velocity (Figure 3c). At that time the surface flow is angled at 45° to the front and the lower layer flow is nearly parallel to the front (5°) (Figure 1). The front and velocity field continue to rotate such that in the middle of the sediment pulse during the peak flux the lower layer transport is offshore and the front is nearly parallel to the coast (Figures 1 and 3f). Toward the end of the sediment pulse the alongshore flow has reversed and the lower layer flow is offshore and upcoast. Here we refer to flow directed alongshore (southwest) toward the river mouth as upcoast. The average direction of the lower layer velocity and sediment flux during the pulse is 107° to the coast, offshore, and slightly upcoast (Figure 1).

The observed peak in SSC cannot be explained by local resuspension; SSC is not correlated with bottom stress during this period and it peaks when the stress is at a minimum (Figure 3e). Nor can it be explained by advection of sediment in the plume layer as the surface (1 m) sediment concentration decreases when the front arrives (Figure 3d). Rather, the pulse of high SSC at the 12 m mooring is always associated with offshore flow in the lower layer (Figure 3b), suggesting that the sediment originates from a source landward of the 12 m mooring. This is shown by example in Figure 3 but is observed for every sediment flux event shown in Figure 2c.

In order to investigate the direction of provenance of sediment transported during the frontal pulse, we estimate trajectories by integrating the sediment flux observed 3 m above the bottom backward in time for 30 min (Figure 1). For example, integration for the initial trajectory (Figure 1; dark blue dashed line) begins at 16:40, shortly after the front passes, and results in the flux observed at the mooring location (Figure 1; dark blue solid arrow) 30 min later at 17:10. Fine sediment with a settling velocity of 1 mm s^{-1} will take

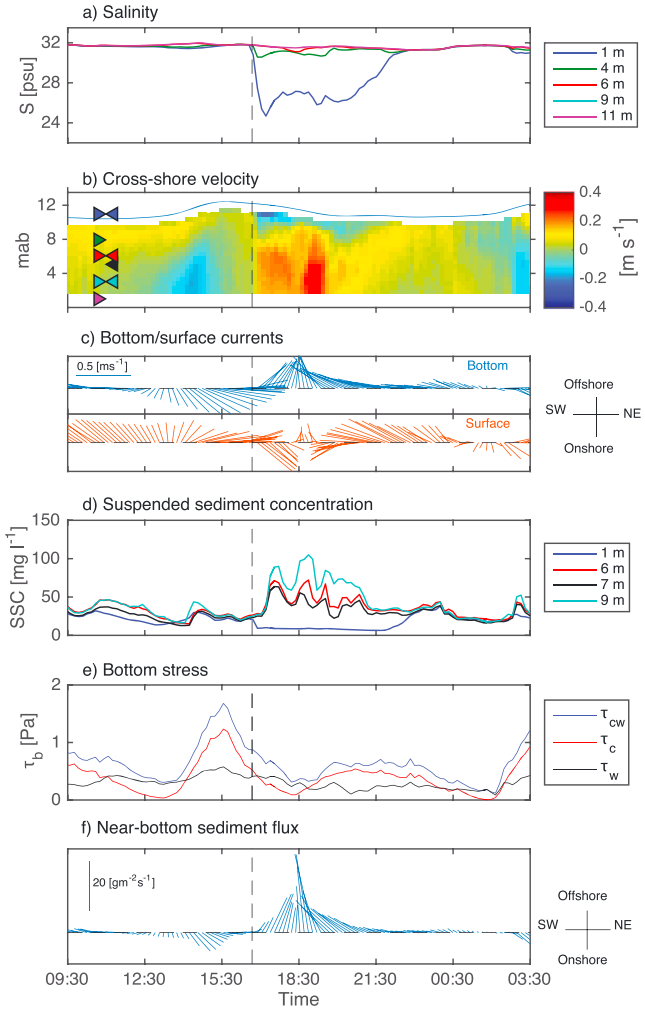

Figure 3. Frontal passage on day 57. (a) Salinity; (b) cross-shore velocity; (c) stick plots of near-surface and near-bottom velocity; (d) sediment concentration; (e) estimated bottom stress due to tidal currents (τ_c), waves (τ_w), and combined waves and currents (τ_{cw}); and (f) near-bottom (3 mab) sediment flux magnitude and direction. The depth of the salinity and sediment sensors is relative to the water surface. The frontal arrival at 16:43 is indicated with a vertical dashed line. Right (left) triangles in Figure 3b indicate the location of the CTD (OBS) sensors at high water with fill colors corresponding to line colors in Figures 3a and 3b, respectively.

approximately 50 min to settle 3 m and will thus stay in suspension for the duration of the computed trajectories. The assumed settling velocity of 1 mm s^{-1} represents an upper bound based on settling velocities estimated during later experiments at the same location (not shown). These trajectories are approximate because they cannot account for the spatial variability in the flow field; however, they provide the best available estimate of the source region for the observed sediment fluxes.

The initial trajectory (17:10) shows that the transport first observed at the mooring originates upcoast (SW) and propagates parallel to the front but results in a relatively small sediment flux. As the front propagates onshore and the current rotates, the trajectories are oriented increasingly perpendicular to the coast and the corresponding sediment flux observed at the mooring increases. By the end of the sediment pulse, the transport direction has rotated more than 90° and sediment flux originates downcoast, carrying sediment southwest past the mooring. The trajectories show that all of the sediment flux originates in the region landward of the mooring.

3.3. Tidal Straining and the Generation of Fronts

It is clear from our measurements that the offshore sediment flux is associated with vertical shear in the cross-shore velocity that develops almost instantaneously after the passage of the freshwater front

(Figures 3b and 3c). Vertical shear is generated under stratified conditions along the Dutch coast due to the decoupling of the surface layer from the lower layer in a process described by *Visser et al.* [1994]. This process generates counterrotating anticyclonic and cyclonic tidal ellipses in the surface and lower layers, respectively, subsequently increasing or decreasing vertical stratification through tidal straining [*Souza and Simpson*, 1996]. It results in seaward flow in the lower layer and landward flow in the upper layer following flood tide, as observed in our measurements. Numerical modeling shows that the elliptical tidal motion advects the Rhine ROFI onshore and offshore each tidal cycle [*De Boer et al.*, 2008], carrying the inner edge of the ROFI past our measurement site shortly after high water. This is consistent with the timing of frontal passage in our measurements and suggests that the observed fronts could be the result of the cross-shore advection of the inner edge of the ROFI.

Alternately, the observed front may be associated with lenses of brackish water that are ejected from the Rhine River mouth on ebb tide, as described by *de Ruijter et al.* [1997], which generate fronts that propagate across the ROFI and are eventually advected with it. Model studies by *De Boer et al.* [2008, 2009] show that multiple fronts generated by the advection of lenses may be present at this midfield site and that the initial ebb front is also likely to arrive shortly after high water.

We expect, therefore, that the shear and sediment transport observed during the frontal period is associated with fronts formed either by the inner edge of the ROFI or the leading edge of an ejected tidal lens, which may be followed by other internal fronts propagating within the plume. The frontal passage initiates strong counterrotating velocities, which drive sediment offshore in the lower layer. The initial pulse of offshore transport may also be enhanced by convergence caused by the alongshore component of the frontal propagation, as described in section 3.2. It is important to note that the transport pulse associated with the frontal events lasts for a few hours, much longer than the initial frontal passage. Thus, the cross-shore currents that are maintained during the subsequent period of stratification are an important component of the transport process. However, the net offshore flux observed during the frontal period is not observed when stratification persists throughout the tidal cycle (Figures 2a and 2c; days 62–64). As shown by *Flores et al.* [2017], periods of sustained stratification are more often associated with onshore sediment flux in the lower layer as a result of the shoreward flow induced by stratification on the opposite phase of the tide.

3.4. The Nearshore as a Source of SSC

A nearshore source of elevated SSC is required to explain the occurrence of elevated SSC at the 12 m site due to advection from farther inshore. No corresponding measurements of SSC closer to shore were made during this experiment. However, turbidity is typically high close to shore due to elevated bottom stresses from waves and tidal currents in the nearshore region. Analysis of bottom sediment shows that the 12 m site consisted primarily of very fine and fine sands and silt, which are predicted to be resuspended when the wave-orbital velocity exceeds approximately 0.25 ms^{-1}. While sediment advected past our mooring likely consists of finer material than sand, resuspension of fine sand mobilizes high concentrations of fines that are bound in the bed. On day 57 the depth contour corresponding to a wave orbital velocity of 0.25 ms^{-1} was 9 m, suggesting that fine sand was resuspended by waves in 9 m or less of water (Figure 2b).

With the exception of the first and last three trajectories, all of the computed trajectories show that sediment observed at the mooring originated at or landward of the 9 m isobath (Figure 1). The first trajectory originates offshore of the 9 m isobath and arrives at the mooring at 17:10, 27 min after the front but before the first peak in SSC. The second trajectory (17:40) originates near the 9 m isobath and corresponds to the first peak in SSC (Figure 3c). The subsequent three trajectories all appear to carry sediment originating landward of the 9 m isobath. While the final three trajectories originate seaward of the 9 m isobath, it is likely that nearshore sediment has been moved offshore all along the coast since the tidal velocity has been directed offshore for the preceding 2 h.

We also find that the sediment concentration observed at the 12 m site is correlated with nearshore wave activity. The mean wave orbital velocity landward of the 12 m mooring (Figure 2b) during a 5 h window centered on each SSC peak is correlated ($r^2 = 0.64$) with the magnitude of the SSC peak (Figure 4a). It is important to note that tidal current stresses are high along the Dutch coast, as documented by the large peak in current stress (τ_c) 1.25 h before the front arrives (Figure 3e). While tidal current stresses likely also contribute to the stress that resuspends sediment in the surf zone and nearshore region, wave stresses are typically significantly higher.

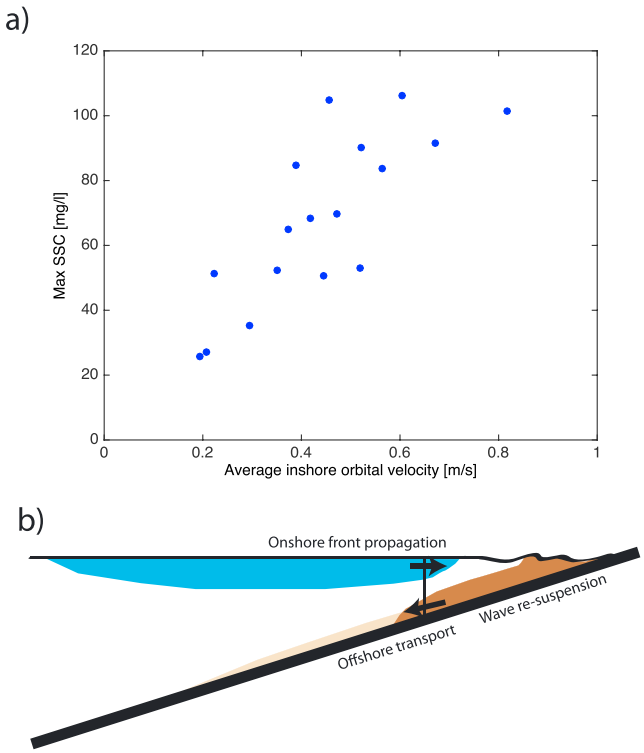

Figure 4. (a) Relationship between observed peak SSC at the 12 m mooring and the average wave orbital velocity inshore of the mooring. (b) Simplified schematic showing how the frontal pumping mechanism generates cross-shore sediment transport. Bottom stress associated with waves resuspends sediment inshore, which is subsequently pumped offshore at depth by the velocity induced by tidal straining of the plume.

The estimated sediment flux trajectories and the correlation of the SSC peaks with nearshore wave orbital velocities support the conclusion that high SSC from the nearshore is the source of sediment for the pulse observed offshore at the 12 m mooring.

4. Discussion

We conclude that the dominant mode of cross-shelf transport observed during this sampling period is due to frontal pumping of nearshore suspended sediment. This involves the interaction of two distinct mechanisms, which are illustrated in Figure 4b. Waves in the nearshore resuspend bottom sediment, out to a depth of approximately 9 m on this day. Plume-generated fronts propagate alongshore and onshore generating counterrotating surface and bottom velocities with strong vertical shear. During the stratified period following frontal passage, the average flow direction in the lower half of the water column is offshore and this pulse of seaward flow carries nearshore suspended sediment offshore. The combination of resuspension due to waves and advection due to baroclinic river plume processes is effective for driving significant cross-shore transport. Resuspension in the energetic nearshore generates high sediment concentrations and sustained cross-shore currents associated with the plume generate transport over large cross-shore distances. Indeed, integration of the observed cross-shore velocity during the high SSC event shows that nearshore sediment can be transported more than 2.5 km offshore by the frontal pumping mechanism described here. This process may thus help to explain the repeated observation that a localized region of elevated turbidity exists 1.5 km to 5 km from the Dutch coast [*Van Alphen*, 1990; *Joordens et al.*, 2001; *van der Hout et al.*, 2015].

Cross-shelf sediment transport by fronts has not been examined in other plume systems, but the main forcing components are often present; many open coastlines are subject to significant wave action capable of suspending available sediment, and plume fronts often generate cross-shore velocities on the order of 0.1 ms^{-1} near the coast [e.g., *Lentz et al.*, 2003; *Mazzini and Chant*, 2016]. However, other characteristics specific to individual systems may also influence this process. For example, the outlet to the ocean of many large rivers including the Rhine are engineered for vessel traffic with the construction of long jetties out into the ocean or

sea. These jetties force the outflowing river water to separate from the coast and, through this process, may increase the probability that plume fronts propagate onshore, as tides, buoyancy or Earth's rotation carry the freshwater back toward the coast. Cross-shore sediment transport in other systems may ultimately be limited by availability of fine sediment, though the physical process described here may also transport other material from the nearshore to the inner shelf.

Finally, it is worth asking whether the Sand Engine directly influences this process due to its potential impact on local hydrodynamics or sediment supply. The computed cross-shore sediment flux during the unstratified period (days 54–56) shows that tidal flow past the Sand Engine creates very little cross-shore transport on its own (Figure 2c), suggesting that the perturbation to the flow does not create significant cross-shore transport on its own. Furthermore, while the emplacement of the Sand Engine undoubtedly provides a large source of sediment, the observed suspended sediment concentrations are in the same range as those observed along the Dutch coast prior to construction of the Sand Engine [e.g., *van der Hout et al.*, 2015]. Thus, while the plume frontal pumping process clearly contributes to offshore flux of fine sediments in the Sand Engine region, the mechanisms associated with this process require neither the bathymetric perturbation nor the excess sediment supply associated with the Sand Engine.

5. Summary

We document a new cross-shore exchange mechanism for sediment driven by the onshore propagation of a river plume front, which penetrates through the nearshore region to the shoreline. In our study site along the Dutch coast, this exchange mechanism is coincident with high sediment resuspension rates in the nearshore and results in significant offshore transport of suspended sediment.

Acknowledgments
The authors would like to thank Chris Balfour and the crew of the R/V *Arca* for their support during the measurements, Ad Stolk and Rijkswaterstaat for their generous in-kind support, and Onno van Tongeren and Wil Borst from the Port of Rotterdam and Marcel Stive from TU Delft. The authors are grateful for support from the Netherlands Organisation for Scientific Research STW program project 12682 Sustainable Engineering of Coastal Systems in Regions of Freshwater Influence and ERC-advanced grant 291206 Nearshore Monitoring and Modeling (NEMO). ARH-D was supported by the Allan and Inger Osberg Professorship. A.J.S. was funded by NERC through NOC's National Capability funding. The data can be made available by contacting the corresponding author (arhd@uw.edu) and will be archived in national data centers in the UK and the Netherlands upon completion of the research project.

References

Burchard, H., H. M. Schuttelaars, and W. R. Geyer (2013), Residual sediment fluxes in weakly-to-periodically stratified estuaries and tidal inlets, *J. Phys. Oceanogr.*, *43*(9), 1841–1861.

De Boer, G. J., J. D. Pietrzak, and J. C. Winterwerp (2008), Using the potential energy anomaly equation to investigate tidal straining and advection of stratification in a region of freshwater influence, *Ocean Modell.*, *22*, 1–11.

De Boer, G. J., J. D. Pietrzak, and J. C. Winterwerp (2009), SST observations of upwelling induced by tidal straining in the Rhine ROFI, *Cont. Shelf Res.*, *29*, 263–277.

de Nijs, M. A., J. C. Winterwerp, and J. D. Pietrzak (2010), The effects of the internal flow structure on SPM entrapment in the Rotterdam waterway, *J. Phys. Oceanogr.*, *40*(11), 2357–2380.

de Ruijter, W. P., A. W. Visser, and W. Bos (1997), The rhine outflow: a prototypical pulsed discharge plume in a high energy shallow sea, *J. Mar. Syst.*, *12*(1), 263–276.

Fewings, M., S. J. Lentz, and J. Fredericks (2008), Observations of cross-shelf flow driven by cross-shelf winds on the inner continental shelf, *J. Phys. Oceanogr.*, *38*(11), 2358–2378.

Flores, R., S. Rijnsburger, A. R. Horner-Devine, A. J. Souza, and J. D. Pietrzak (2017), The impact of storms and stratification on sediment transport in the Rhine region of freshwater influence, *J. Geophys. Res. Oceans*, doi:10.1002/2016JC012362.

Fredsøe, J., and R. Deigaard (1992), *Mechanics of Coastal Sediment Transport*, vol. 3, World Sci., Singapore.

Garvine, R. W. (1974), Dynamics of small-scale oceanic fronts, *J. Phys. Oceanogr.*, *4*, 557–569.

Grant, S. B., J. H. Kim, B. H. Jones, S. A. Jenkins, J. Wasyl, and C. Cudaback (2005), Surf zone entrainment, along-shore transport, and human health implications of pollution from tidal outlets, *J. Geophys. Res.*, *110*, C10025, doi:10.1029/2004JC002401.

Grant, W. D., and O. S. Madsen (1979), Combined wave and current interaction with a rough bottom, *J. Geophys. Res.*, *84*(C4), 1797–1808.

Horner-Devine, A., R. D. Hetland, and D. MacDonald (2015), Transport and mixing in coastal river plumes, *Annu. Rev. Fluid Mech.*, *47*, 569–594.

Joordens, J., A. Souza, and A. Visser (2001), The influence of tidal straining and wind on suspended matter and phytoplankton distribution in the rhine outflow region, *Cont. Shelf Res.*, *21*(3), 301–325.

Kilcher, L., and J. Nash (2010), Structure and dynamics of the Columbia River tidal plume front, *J. Geophys. Res.*, *115*, C05S90, doi:10.1029/2009JC006066.

Lentz, S. J., and M. R. Fewings (2012), The wind-and wave-driven inner-shelf circulation, *Annu. Rev. Mar. Sci.*, *4*, 317–343.

Lentz, S. J., S. Elgar, and R. Guza (2003), Observations of the flow field near the nose of a buoyant coastal current, *J. Phys. Oceanogr.*, *33*(4), 933–943.

Mazzini, P. L., and R. J. Chant (2016), Two-dimensional circulation and mixing in the far field of a surface-advected river plume, *J. Geophys. Res.*, *121*, 3757–3776, doi:10.1002/2015JC011059.

Ohlmann, J. C., M. R. Fewings, and C. Melton (2012), Lagrangian observations of inner-shelf motions in southern california: Can surface waves decelerate shoreward-moving drifters just outside the surf zone?, *J. Phys. Oceanogr.*, *42*(8), 1313–1326.

Pietrzak, J. D., G. J. de Boer, and M. A. Eleveld (2011), Mechanisms controlling the intra-annual mesoscale variability of SST and SPM in the southern North Sea, *Cont. Shelf Res.*, *31*(6), 594–610.

Reniers, A. J., J. MacMahan, E. Thornton, T. Stanton, M. Henriquez, J. Brown, J. Brown, and E. Gallagher (2010), Surf zone surface retention on a rip-channeled beach, *J. Geophys. Res.*, *114*, C10010, doi:10.1029/2008JC005153.

Rilov, G., S. E. Dudas, B. A. Menge, B. A. Grantham, J. Lubchenco, and D. R. Schiel (2008), The surf zone: A semi-permeable barrier to onshore recruitment of invertebrate larvae?, *J. Exp. Mar. Biol. Ecol.*, *361*(2), 59–74.

Shanks, A. L., S. G. Morgan, J. MacMahan, and A. J. Reniers (2010), Surf zone physical and morphological regime as determinants of temporal and spatial variation in larval recruitment, *J. Exp. Mar. Biol. Ecol.*, *392*(1), 140–150.

Souza, A., and J. Simpson (1996), The modification of tidal ellipses by stratification in the Rhine ROFI, *Cont. Shelf Res.*, *16*(8), 997–1007.

Stive, M., and J. A. Battjes (1984), A model for offshore sediment transport, in *Proceedings of the 19th International Conference Coastal Engineering*, pp. 1420–1436, Am. Soc. of Civ. Eng., Houston, Tex.

Stive, M. J., M. A. de Schipper, A. P. Luijendijk, S. G. Aarninkhof, C. van Gelder-Maas, J. S. van Thiel de Vries, S. de Vries, M. Henriquez, S. Marx, and R. Ranasinghe (2013), A new alternative to saving our beaches from sea-level rise: The Sand Engine, *J. Coastal Res.*, *29*(5), 1001–1008.

Van Alphen, J. (1990), A mud balance for Belgian-Dutch coastal waters between 1969 and 1986, *Neth. J. Sea Res.*, *25*(1–2), 19–30.

van der Hout, C. M., T. Gerkema, J. J. Nauw, and H. Ridderinkhof (2015), Observations of a narrow zone of high suspended particulate matter (SPM) concentrations along the Dutch coast, *Cont. Shelf Res.*, *95*, 27–38.

Visser, A., A. Souza, K. Hessner, and J. Simpson (1994), The effect of stratification on tidal current profiles in a region of fresh-water influence, *Oceanolog. Acta*, *17*(4), 369–381.